JOURNAL OF VIROLOGY, Jan. 2004, p. 302–313 Vol. 78, No. 1
0022-538X/04/$08.00+0 DOI: 10.1128/JVI.78.1.302–313.2004

Selectively Receptor-Blind Measles Viruses: Identification of Residues Necessary for SLAM- or CD46-Induced Fusion and Their Localization on a New Hemagglutinin Structural Model

Sompong Vongpunsawad,[1] Numan Oezgun,[2] Werner Braun,[2] and Roberto Cattaneo[1]*

Molecular Medicine Program, Mayo Clinic, and Virology and Gene Therapy, Mayo Graduate School, Rochester, Minnesota 55095,[1] and Sealy Center for Structural Biology, University of Texas Medical Branch, Galveston, Texas 77555[2]

Received 22 July 2003/Accepted 23 September 2003

Measles virus (MV) enters cells either through the signaling lymphocyte activation molecule SLAM (CD150) expressed only in immune cells or through the ubiquitously expressed regulator of complement activation, CD46. To identify residues on the attachment protein hemagglutinin (H) essential for fusion support through either receptor, we devised a strategy based on analysis of morbillivirus H-protein sequences, iterative cycles of mutant protein production followed by receptor-based functional assays, and a novel MV H three-dimensional model. This model uses the Newcastle disease virus hemagglutinin-neuraminidase protein structure as a template. We identified seven amino acids important for SLAM- and nine for CD46 (Vero cell receptor)-induced fusion. The MV H three-dimensional model suggests (i) that SLAM- and CD46-relevant residues are located in contiguous areas in propeller β-sheets 5 and 4, respectively; (ii) that two clusters of SLAM-relevant residues exist and that they are accessible for receptor contact; and (iii) that several CD46-relevant amino acids may be shielded from direct receptor contacts. It appears likely that certain residues support receptor-specific H-protein conformational changes. To verify the importance of the H residues identified with the cell-cell fusion assays for virus entry into cells, we transferred the relevant mutations into genomic MV cDNAs. Indeed, we were able to recover recombinant viruses, and we showed that these replicate selectively in cells expressing SLAM or CD46. Selectively receptor-blind viruses will be used to study MV pathogenesis and may have applications for the production of novel vaccines and therapeutics.

Measles, caused by wild-type measles viruses (MVs), is one of the leading causes of infant death in developing countries (11). The immune suppression that accompanies measles significantly enhances an individual's susceptibility to secondary infections, and these infections account for most of the morbidity and mortality (4). Vaccination with the live attenuated strain Edmonston (MV-Edm) prevents measles-related fatalities and only rarely results in the development of mild symptoms (17). Cell entry likely plays a central role in MV pathology: most wild-type MV strains preferentially use the immune-cell-specific protein SLAM as a receptor (19, 27, 51, 80), whereas MV-Edm enters cells more efficiently using the ubiquitous protein CD46 (16, 47, 72). Since the three morbilliviruses—MV, canine distemper virus (CDV), and rinderpest virus (RV)—enter cells through SLAM (human, canine, or bovine) and are immunosuppressive (81), SLAM-dependent cell entry may be directly related to pathogenesis; CD46 interactions have also been correlated with immunosuppression (32, 37, 50).

The attachment protein of morbilliviruses has hemagglutination but not neuraminidase activity and is therefore named hemagglutinin (H) rather than HN (hemagglutinin-neuraminidase). H is a type II transmembrane glycoprotein that dimerizes in the endoplasmic reticulum (58, 67). After binding to the receptor, it supports fusion of the viral and cellular membranes by inducing a conformational change of the trimeric fusion (F) protein (10, 85). No information on the morbillivirus H-protein structure is available, but a model based on the structure of the influenza virus neuraminidase and an intermediate model of a paramyxovirus HN has been presented by Langedijk et al. (35). Since the crystal structure of a paramyxovirus HN protein has recently been determined (13), a more reliable three-dimensional model of MV H can now be generated.

To generate this model, we relied on our procedure based on distance geometry in torsion angles and energy refinement with the program FANTOM (44, 65, 69, 76–78). In this procedure the alignment between template and target sequence is examined for consistency of secondary structure and sequence motif. Recently, we added a new feature for the identification of motifs with conserved physical-chemical properties in a family of sequences (39, 70, 83, 88), available online at http://www.scsb.utmb.edu/masia/masia.html. The three-dimensional models we generated in the past provided valuable guidance for mutagenesis studies for several proteins, including the two external domains of the MV receptor CD46 (24, 40, 45, 46, 70, 78, 87). The three-dimensional model of CD46, which was based on a template with <25% sequence identity, was later confirmed by the crystal structure (7).

The paramyxovirus attachment proteins are involved not only in receptor binding but also in transducing the fusion-inducing signal from the receptor to the F protein (41, 79). Limited information is available on the MV H-protein residues important for receptor binding or fusion support. Sequence examination of the H genes of different MV strains indicated that positions 451 and 481 are at variance between wild-type

* Corresponding author. Mailing address: Molecular Medicine Program, Mayo Clinic, Guggenheim 18, 200 First St., SW, Rochester, MN 55905. Phone: (507) 284-0181. Fax: (507) 266-2122. E-mail: cattaneo.roberto@mayo.edu.

strains on one side and attenuated strains on the other. These two positions were shown to be critical for determining the ability of MV strains to cause hemabsorption, cell fusion, and CD46 downregulation (3, 36). One of these amino acids, Y481 (one-letter amino acid code), strongly influences the efficiency of CD46 binding in a baculovirus-infected-cell-based binding assay (28). Nevertheless, a recombinant virus with a wild-type H-protein N481 residue does propagate in Vero cells (31), suggesting either that Y481 is not an absolute requirement for CD46 binding or that a second receptor exists on Vero cells (25). Other studies identified amino acids 473 to 477 as another site required for CD46 interactions (53) and amino acids 548 to 549 as a site required for CD46 downregulation (38). Moreover, residue 546 is at variance between different strains, and it has been suggested that it may play a role in virus adaptation to different growth conditions (30, 62, 75). No information about the H residues relevant for SLAM-mediated entry has been published yet.

To identify residues selectively important for SLAM or CD46 binding or subsequent fusion-related events without resorting to saturating mutagenesis of single amino acids, we devised a strategy relying initially on mutagenesis of blocks of residues. Based on the observations that MV, CDV, and RV interact with SLAM, whereas only MV uses CD46 as a receptor, we mutated blocks of conserved or diverging amino acids, respectively. We then quantified the fusion-support function of the mutants by using two receptor-dependent cell fusion assays. Certain mutants selectively lost function either in CHO cells expressing SLAM or in Vero cells that naturally express CD46. Single amino acid mutants were then produced and tested; the analysis was completed with an additional mutagenesis round based on the new MV H-protein structural model. We characterized 16 residues important for receptor-dependent H-protein fusion promotion and predicted their location on the model. The relevance of certain H residues identified with the cell-cell fusion assay for virus entry into cells was confirmed after transfer of the relevant mutations into an infectious MV cDNA and recovery of the recombinant viruses.

MATERIALS AND METHODS

Cells and viruses. Vero (African green monkey kidney) cells were maintained in Dulbecco modified Eagle medium (DMEM) supplemented with 5% fetal bovine serum (FBS). B95a (a marmoset B-cell line kindly provided by D. Gerlier) was maintained in DMEM and 10% FBS. The rescue helper cell line 293-3-46 (60) was grown in DMEM with 10% FBS and 1.2 mg of G418/ml. Vero-SLAM and CHO-SLAM (cells expressing human signaling lymphocyte activation molecules [kindly provided by Y. Yanagi]) were maintained in DMEM supplemented with 10% FBS and 0.5 mg of G418/ml or RPMI 1640 medium supplemented with 10% FBS and 0.5 mg of G418/ml, respectively.

Plasmids and expression studies. For the fusion experiments, cells were seeded on 24-well tissue culture plate without antibiotics and allowed to reach ~80% confluence prior to transfection. Equal amounts (1 μg) of pCG-F (8) and the mutated pCG-H were transfected into the cells by using Lipofectamine 2000 (Invitrogen) according to the manufacturer's protocol. Briefly, 2 μl of Lipofectamine 2000 was diluted in 50 μl of Opti-MEM, mixed, and incubated at room temperature for 5 min. Meanwhile, plasmid DNAs were diluted in 50 μl of Opti-MEM. The two solutions were combined, mixed, and incubated for 20 min before they were added to the cells. Cells were analyzed 24 to 48 h posttransfection, and the fusion effect was quantified after we observed the whole surface of the well. The extent of fusion was reported by using the following notation: 0 (empty bars/rectangles), no syncytium found; 1 (one-third filled), syncytia found in some fields of view; 2 (two-thirds filled), syncytia found in most fields of view; and 3 (completely filled), the majority of the cells in the well were either in syncytia or had already detached from the plate because of extensive cell fusion. An average fusion score was assigned for each mutant after at least three independent experiments.

Construction, recovery, and analysis of recombinant viruses. Selected H mutants were transferred into the infectious MV genome by moving the *Pac*I/*Spe*I fragment containing the H open reading frame from pCG-H into *Pac*I/*Spe*I-digested p(+)MVeGFP. This plasmid encodes a MV genome with an enhanced green fluorescent protein (GFP) gene inserted in additional transcription unit situated upstream of the N gene (18). All engineered MV genomes were of hexameric length (61). The Edmonston B-based parental MV strain and all its recombinant derivatives were rescued basically as described previously (60). To prepare virus stocks, Vero or Vero-SLAM cells were infected at a multiplicity of infection (MOI) of 0.01 and then incubated at 37°C. Cells were scraped into Opti-MEM I reduced-serum medium (Invitrogen) and freeze-thawed once. Titers were determined by 50% tissue culture infective dose titration on either Vero or Vero-SLAM cells. For the comparative analysis of the infections of recombinant viruses, cells were washed once with phosphate-buffered saline and infected at an MOI of 0.1 in Opti-MEM for 2 h at 37°C. Fluorescence microscopy photographs were taken at 30 h postinfection for Vero and at 48 h postinfection for B95a cells.

Immunoblotting. Cells were infected with the recombinant or the control viruses at the MOI of 0.1. At the appropriate time they were disrupted by the addition of lysis buffer (50 mM Tris [pH 8.0], 62.5 mM EDTA, 1% IGEPAL CA-630 [formerly NP-40], 0.4% deoxycholate; Sigma) supplemented with Complete protease inhibitor (Roche Biochemicals), and the lysates were clarified by centrifugation at 1,300 × *g* for 10 min at 4°C. The total protein concentration of the cell extracts was determined by using the DC protein assay kit (Bio-Rad). Equal amounts of proteins from cell extracts were denatured for 5 min at 95°C in Laemmli sample buffer (Bio-Rad) containing 10% β-mercaptoethanol, fractionated on sodium dodecyl sulfate—7.5% polyacrylamide gels (Bio-Rad), and blotted onto polyvinylidene difluoride membranes (Millipore). The membranes were blocked with 10% skim milk powder in PBST (1.54 mM KH_2PO_4, 155.17 mM NaCl, 2.71 mM Na_2HPO_4 [pH 8.0] [Invitrogen], 0.1% Tween 20) for 1.5 h at room temperature. The membranes were then incubated with rabbit anti-H cytoplasmic tail antiserum diluted 1:5,000 (9). After incubation with peroxidase-conjugated goat anti-rabbit immunoglobulin G (Jackson Immunoresearch) for 45 min at room temperature, proteins were visualized by enhanced chemiluminescence (Amersham Pharmacia Biotech).

H-protein structure modeling. Modeling of MV H was done according to a standard eight-step procedure (39, 44, 65, 69, 76–78, 86). (i) Sequences related to the target sequence were collected, and a multiple alignment was generated. (ii) By using this multiple alignment, a list of conserved motifs was generated. (iii) A secondary structure prediction for the target sequence was formulated. (iv) The target sequence was submitted to different fold recognition servers to get alignments with the existing protein data base (PDB) structures. (v) The fold recognition server alignments were evaluated and improved, if necessary, to get a final alignment. (vi) A model with the alignment(s) and the corresponding PDB structure(s) was generated as a template. (vii) The quality of the model was evaluated. (viii) Finally, the model was energy minimized.

For step i, we conducted a BLASTP/PSI BLAST (1, 68) search and then used the taxonomy report to identify representative members of the sequence families close to the MV H target sequence. We collected the sequences of hemagglutinin (RV [gi:4468967]), hemagglutinin (peste-des-petits-ruminants virus [gi:1648928]), structural viral protein (dolphin morbillivirus [gi:974809]), viral structural protein (CDV [gi:1149612]), and hemagglutinin (phocine distemper virus [gi:94036]). The gi numbers are unique identification codes of the sequences in the NCBI database (http://www.ncbi.nlm.nih.gov/).

Together with the target and these representative sequences, we prepared a multiple alignment by using CLUSTAL W (26, 82). We analyzed the multiple alignment further with MASIA (88), a novel physical-chemical-based web tool (http://www.scsb.utmb.edu/masia/masia.html) (39, 83), and identified 18 motifs. A secondary structure prediction of the target was obtained from JPred (http://www.compbio.dundee.ac.uk/~www-jpred/) (14, 15).

Next, we submitted the target sequence to different fold recognition servers. The HN structure of Newcastle disease virus (NDV) was consistently returned as the most homologous structure. We combined the alignments returned by the fold recognition server 3D-PPSM (http://www.sbg.bio.ic.ac.uk/~3dpssm/html/ffrecog_simple.html) (33) and Bioingbu (http://www.cs.bgu.ac.il/~bioinbgu/form.html) (20) to get a final alignment which fits best the predicted secondary structure of the target to the secondary structure of the template and has high scores for the corresponding motif regions (39). Based on the final alignment, we generated a model with our modeling package MPACK. MPACK combines the programs EXDIS (76), which extracts distance and angle constraints from the template and DIAMOD (65), which generates models by using the geometric

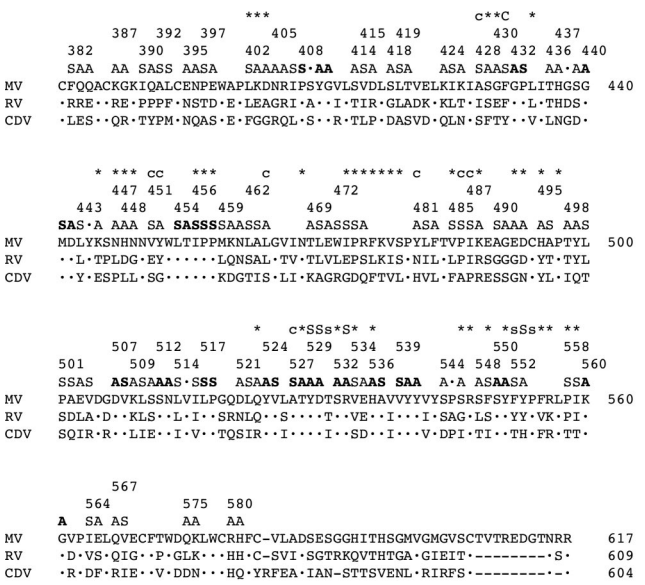

FIG. 1. Sequences of parts of three morbillivirus H proteins and structure of the 60-block mutants produced. The MV, RV, and CDV sequences are shown. The MV H sequence is shown in full; dots are used in the RV and CDV sequences to indicate conserved residues. The three lines above the MV sequence are used to define the 60-block mutants. Two series of mutants were produced: the first included 16 blocks of conserved residues (in boldface), the second 44 blocks of divergent residues (in lightface). Alanine (A) was used to replace charged and polar residues, and serine (S) was used to replace apolar residues. The position of the first amino acid of each block mutant is indicated by an ordinal number. In the top line, the positions of the 56 single amino acid mutants are indicated with an asterisk or a letter. A capital "C" or "S" indicates residues whose mutation completely abolished CD46- or SLAM-dependent fusion support, respectively; a lowercase "c" or "s" indicates residues whose mutation caused strong or moderate reduction in specific receptor-dependent fusion support. All other mutants are indicated by asterisks.

constraint from EXDIS and other sources. Finally, we energy minimized the model with FANTOM (69). We generated all figures of the model with MOLMOL (34).

RESULTS

Construction and characterization of a collection of multiple-residue mutants. To gain insights in H-protein residues important for receptor-dependent fusion promotion, we devised an iterative mutagenesis protocol linked to assays measuring SLAM- or CD46-dependent fusion. We initially focused our mutagenesis on about half of the ectodomain based on following criteria. We excluded amino acids 59 to 154 because they are part of the dimerization stem (58) and thus may be located away from the solvent-exposed surface. We also excluded amino acids 583 to 617 that are deleted in several wild-type strains (52). Knowing that residues important for MV H hemagglutination are located between amino acids 451 and 546 (36, 75), we concentrated initially on amino acids 382 to 582.

Based on a three-way comparison of the MV, RV, and CDV H-protein sequences, we designed 60 mutants covering blocks of two to four amino acids (Fig. 1). Two series of mutants were produced: the first included 16-residue blocks conserved between MV, RV, and CDV (Fig. 1, boldface S and A), the second 44 blocks of divergent residues (Fig. 1, lightface S and A). Mutations of the conserved or divergent residue blocks were candidates for eliciting SLAM- or CD46-dependent effects, respectively. The position of the first mutated amino acid in each block is indicated with an ordinal numeral in Fig. 1. Two small amino acids—alanine to substitute charged and polar residues and serine to replace apolar residues—were used to limit structural interferences, leading to reduced protein folding and transport. Conserved cysteine and tryptophan residues were not mutated to preserve the protein structure and hydrophobic core. After mutagenesis, we confirmed that all of the clones had the expected sequence around the mutagenesis site and that all of the proteins had the expected size.

We then verified the function of all 60 H-protein expression clones in a fusion support test based on the complementation of the standard F protein for its ability to fuse cells. These tests were performed in rodent cells expressing SLAM but not CD46 (CHO-SLAM cells) or simian cells expressing the opposite combination of MV receptors (Vero cells). The efficiency with which all of the mutants fused CHO-SLAM or Vero cells was measured and is represented by small rectangles in Fig. 2. The most informative mutants were those that selectively lost fusion support efficiency with one receptor. Five that lost at least two levels of efficiency in Vero cells are labeled with an asterisk in the upper row of Fig. 2: mutants 402LKD/SAA, 430GF/AS, 451VY/SA, 456IPP/SSS, and 527AT/SA from left to right. Four different mutants lost two levels or more of efficiency on CHO-SLAM cells: 485VP/SS, 529YD/AA, 532SR/AA, and 552FY/SA (Fig. 2, second row from top, mutants with an asterisk). The levels of fusion efficiency were defined semiquantitatively as described in Materials and methods.

Of the remaining 51 mutants tested, 21 maintained full fusion support on both cell lines, 13 completely lost it, and 4 partially lost function at the same level in both cell lines, for a total of 38 "block" mutants that did not discriminate between the receptors. The remaining 13 mutants lost one level of activity: 8 in Vero cells and 5 in CHO-SLAM cells. Many of the proteins that completely lost their function with both receptors were detected at very low levels in cell extracts, suggesting instability (data not shown).

Identification of single amino acids is important for fusion support. We then focused on the nine block mutants yielding the most striking differential fusion efficiencies and produced single amino acid mutants covering all of the positions originally mutated in the blocks. The positions of these and other single amino acids mutants (see below) and the results of the functional tests are shown in Fig. 2 (lower half). For the Vero cell fusion-reduced mutants, position 431 in block 430GF/AS was found to be crucial; both residues 451 and 452 contributed to the effect of 451VY/SA, and only residue 527 was important in 527AT/SA (Fig. 2, lower half, Vero row). In contrast, none of the single mutants in 402LKD/SAA and 456IPP/SSS lost function in Vero cells. Moreover, as a control we mutated Y 481 to A. Even if mutant 481YLF/ASA had lost function in both cell lines (Fig. 2, upper half), 481Y/A retained function selectively in CHO-SLAM cells, as expected. Thus, residues 431, 451, 481, and 527 were identified (shown with their num-

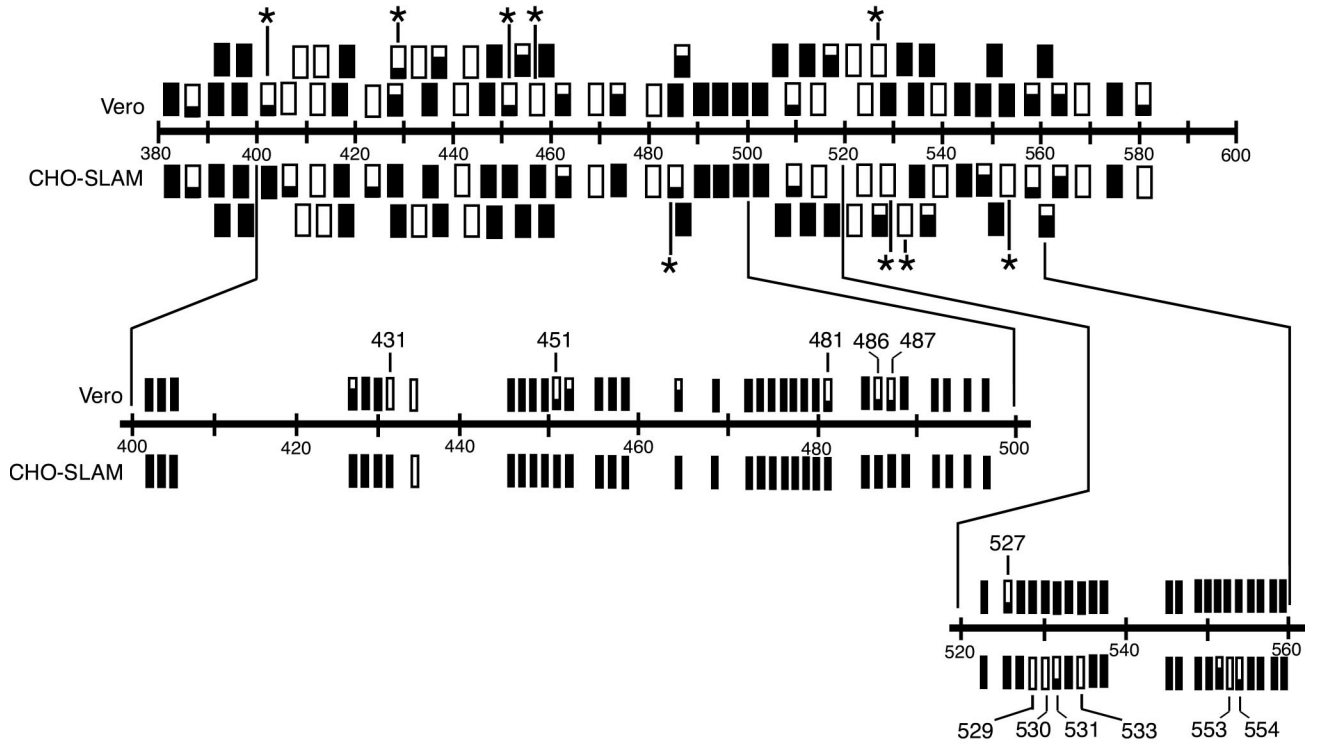

FIG. 2. Fusion efficiency of the H-protein mutants in Vero or CHO-SLAM cells. The 60 H-protein block mutants are represented as rectangles in the top half, and the 56 single residue mutants are shown as bars in the bottom half. A filled rectangle or bar indicates full fusion activity, a void rectangle or bar indicates no fusion activity, and two-thirds- and one-third-filled objects indicate intermediate fusion levels as defined in Materials and Methods. The mutants are drawn according to their ordinal position in the linear H sequence. Block mutants with strong receptor-mediated fusion differential are highlighted with asterisks (upper half); single-residue mutants with strong receptor-mediated fusion differential are indicated by the ordinal numbers corresponding to their positions (lower half).

ber in Fig. 2, lower half, Vero row). These residues served as starting points (anchors) for the next round of mutagenesis.

Single amino acids crucial for fusion were identified also in the CHO-SLAM cell fusion-reduced block mutants. Both positions 529 and 530 of mutant 529YD/AA completely abolished function; in mutant 532SR/AA only position 533 was found to be important, and in mutant 552FY/SA position 553 was found to be crucial, with a smaller effect contributed by residue 552. We thus selected residues 529, 530, 533, and 553 as anchors for the next round of mutagenesis (shown with their number in Fig. 2, lower half, SLAM row). A mutant derived from the last CHO-SLAM cell fusion-reduced block (485VP/SS) produced an unexpected result: position 486 lost function selectively in Vero cells.

New H-protein structural model. We then sought to identify amino acids important for CD46- or SLAM-dependent fusion support located near the anchor residues. Since no high-resolution information on the morbillivirus H-protein structure is available, we therefore constructed a structural model of MV H.

The modeling procedure was based on fold recognition server alignments of the target sequence to experimentally known structures, secondary structure prediction, and scores of motifs generated from a multiple alignment sequence similar to the target sequence. In our case, the sequences of the H proteins of six morbilliviruses (see Materials and Methods) were aligned, and 18 structural motifs were identified (Fig. 3, blocks named a to r in the lines labeled MASIA). The secondary structure of MV H was predicted by using the JPred server, and alignments of MV H to potential templates were obtained from different fold recognition servers. The HN structure of NDV was consistently returned as the best homologous structure. The alignment was then optimized to fit best the predicted secondary structure of the target (Fig. 3, line MV H) to that of the template (Fig. 3, line NDV HN) and to increase the scores of the motifs. This alignment is consistent with the one proposed by Langedijk et al. (35) only between MV residues S250 and C300 and two other short stretches. Based on the new alignment a model was generated and then energy minimized (see Materials and Methods).

This model is shown in Fig. 4A and B, as a ribbon plot, and in Fig. 4C and D as a space-filling model of Corey, Pauling, and Kaltun. The same nomenclature as introduced by Crennell et al. (13) for the NDV HN protein is used for the secondary structure. The globular head of the protein is predicted to consist of a superbarrel in which six β-sheets (sheets 1 to 6) are arranged cyclically around an axis like the blades of a propeller, and loops protrude from the top and lower surfaces of each "blade." Panels A and C are a view of the protein from the top, in panels B and D the model was rotated in mathematically positive direction by 270° around the *x* axis, exposing sheets 4 and 5. This arrangement was chosen to best visualize the residues identified above as being crucial for receptor interactions. In Fig. 4C and D, all residues that have been mutated in

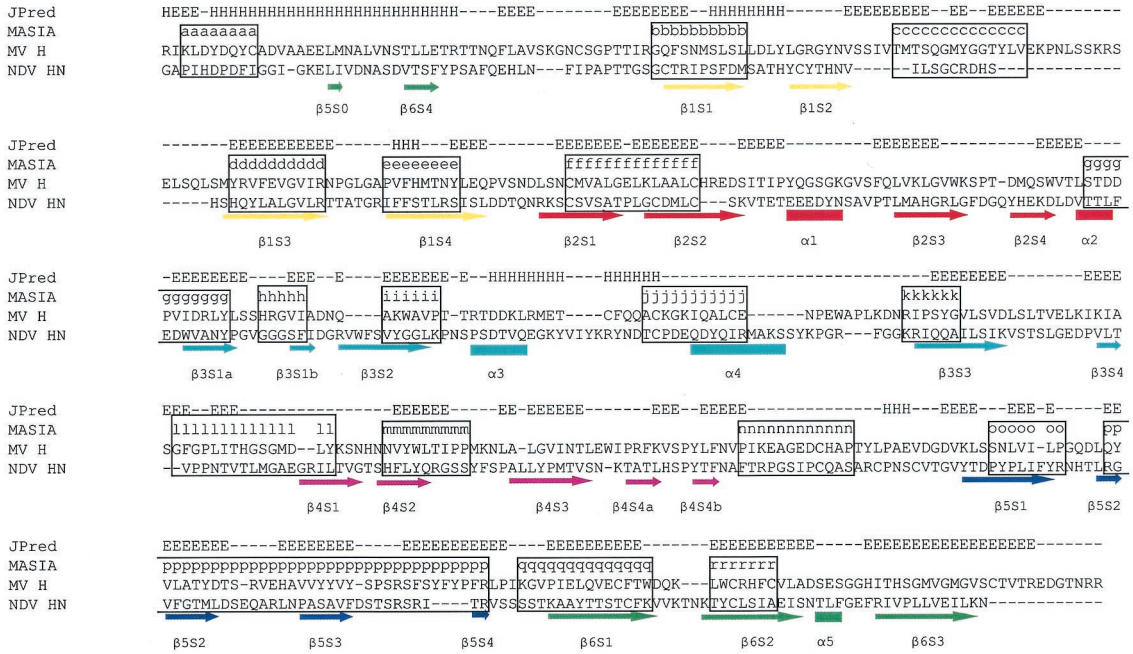

FIG. 3. Alignment of the MV H with the NDV HN protein sequences and secondary structure predictions used for modeling. The 18 secondary structure motifs identified with the program MASIA are indicated above the MV H sequence with a letter (a to r) and boxed. On the top line the results of the JPred structure prediction of H are shown. The secondary structure of the template is shown below the NDV sequence: arrowed lines indicate β-sheets and boxes indicate alpha-helical regions. The structures are color coded according to each of the six predicted "propeller" sheets from 1 to 6: yellow, red, cyan, pink, blue, and green, respectively.

blocks are shown in avocado green; all of the individually mutated amino acids are shown in light blue and are numbered. From this representation it becomes evident that most solvent-exposed residues in the relevant half of the H-protein ectodomain (β-sheets 4 to 6) have been mutated. Seven of the eight anchor residues are predicted to be solvent exposed; only residue 451 is not available for contacts on the protein surface, but modification of this residue to S introduces a consensus glycosylation site NXS at asparagine 449, a residue predicted to be on the surface of the molecule; the predicted new glycosylation site is used (data not shown).

Identification of additional amino acids important for fusion support. We then used the new model to identify solvent-exposed amino acids which alpha-carbon atoms are located within 10 Å of those of the anchor residues. As detailed in Table 1, 30 amino acids conformed to these parameters: 13 surface residues near the CD46 anchors, 15 residues near the SLAM anchors, and 2 residues near both the CD46 and SLAM anchors (I487 and R547). We then mutated these residues and tested their function in CHO-SLAM and Vero cells. Most of the mutated proteins completely maintained their function, with the following exceptions: I487S almost completely lost it selectively in Vero cells, A428S and L464A function was slightly impaired in Vero cells, and T531A and P554S almost completely lost function selectively in CHO-SLAM cells. Thus, mutation of five amino acids predicted to be located near the anchors resulted in partial loss of function selectively with the corresponding receptor.

In Fig. 5 the predicted location of all of the H-protein amino acids for which mutation results in reduction or inactivation of receptor-dependent fusion support, including the anchors, is illustrated. In the discussion below we do not always explicitly indicate that all of the locations we are discussing are hypothetical because they are based on a model; however, this fact should be kept in mind.

Figure 5A and B show the predicted locations of the amino acids that are important for function in CHO-SLAM cells, and Fig. 5C and D show those residues that are important for function in Vero cells. As in Fig. 4, the left panels show top views of the H molecule, the right panels side views. The residues whose mutation abolished SLAM-dependent fusion are shown in red (Y529, D530, R533, and Y553); those whose mutation strongly or moderately impaired SLAM-dependent fusion are shown in gold (T531, F552, and P554, Fig. 5A and B). The only residue whose mutation abolished CD46 (Vero cell)-dependent fusion is pink; those residues whose mutation strongly or moderately impaired CD46-dependent fusion function are dark blue (A428, L464, Y481, I487, and A527; Fig. 5C and D). Two other residues, V451 and P486, strongly impaired CD46-dependent fusion; V451 is predicted to be located below the solvent-exposed surface, but its mutation to S may result in glycosylation of the surface-exposed N449 residue; P486 is also buried and is located close to I487. Finally, Y452 that moderately impaired CD46-dependent fusion is also buried. Thus, according to the model, three of the nine residues interfering with CD46-dependent fusion are not solvent exposed; in contrast, all seven SLAM-relevant residues are on the protein surface.

The SLAM-relevant residues are predicted to be clustered in space: groups of four and three residues located in β-sheet

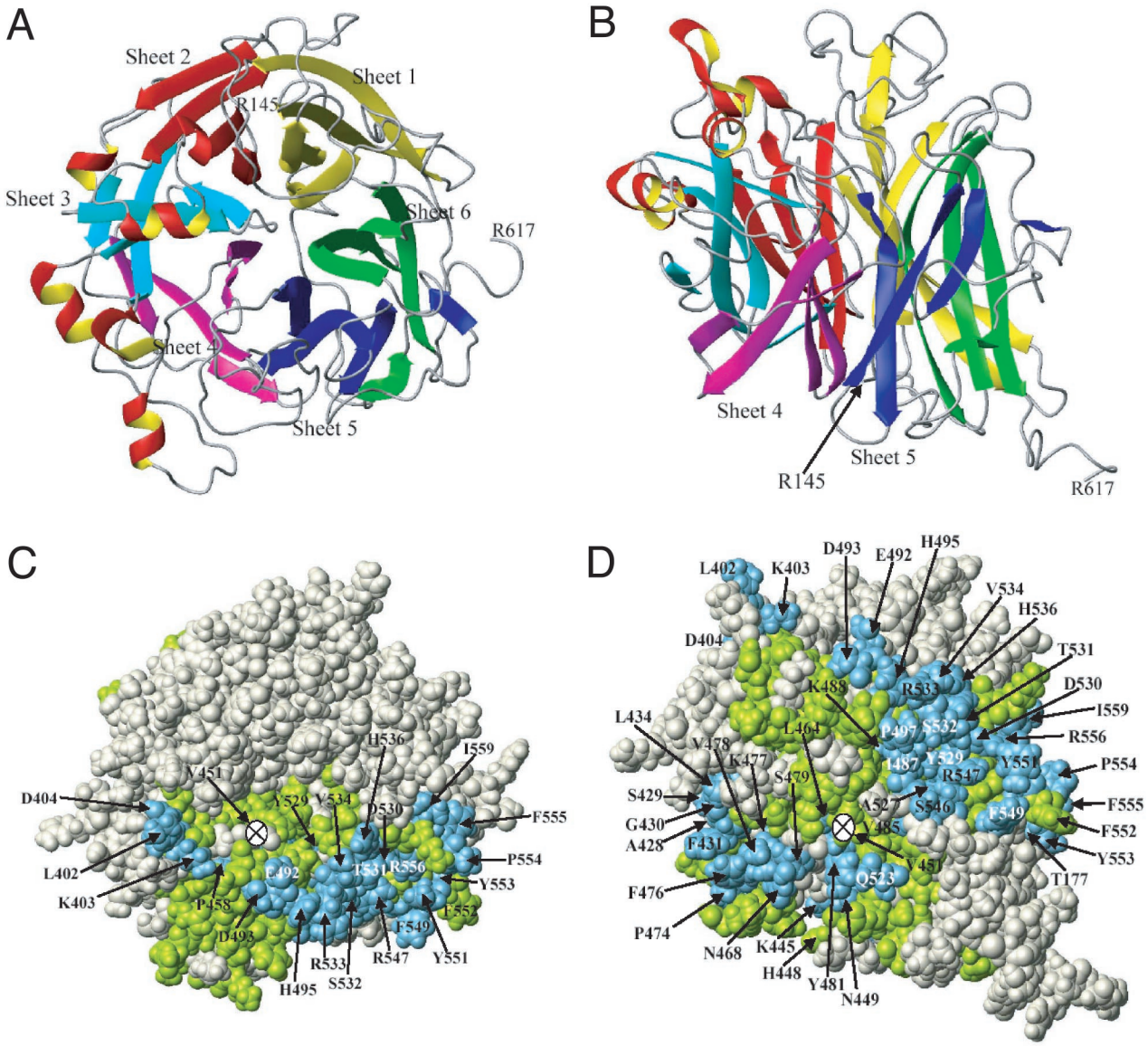

FIG. 4. New MV H-protein structural model showing both ribbon plot (A and B) and space-filling (C and D) representations. Panels A and C are a view of the protein from the top; in panels B and D the model was rotated 270° in a mathematically positive direction around the *x* axis. The same nomenclature as introduced for the NDV HN protein is used here. The globular head of the protein is predicted to consist of a superbarrel in which six β sheets (sheets 1 to 6) are arranged cyclically around an axis like the blades of a propeller and loops protrude from the top and lower surfaces of each "blade." The color code used in panels A and B is the same as that used in Fig. 3. In panels C and D, all residues that have been mutated in blocks are shown in avocado green; all of the individually mutated amino acids are shown in light blue and have been numbered. Residues indicated in gray were not mutated.

5 (Fig. 5A and B). Not all CD46-relevant residues are solvent exposed and thus visible in Fig. 5C and D, but when all residues are considered, three clusters are formed: (i) A527, I487, and P486; (ii) Y481, L464, Y452, and V451; and (iii) F431 and A428. One residue cluster is located at the interface of β-sheets 4 and 5, near one of the SLAM-relevant clusters (Fig. 5C and D). The other two clusters are located in β-sheet 4. According to the model, all CD46-relevant residues are situated in a large belt below the midline of the protein head.

It is noteworthy that four of the seven residues important for SLAM-dependent fusion are conserved among all three morbilliviruses considered, and two are conserved among MV and RPV (Fig. 1, upper line). On the other hand, eight of the nine residues important for CD46-dependent fusion diverge. Thus, the initial assumption in our mutagenesis strategy was correct.

Production and characterization of selectively receptor-blind viruses. The experiments presented above were based on the transient expression of mutated H proteins and on the quantification of their receptor-dependent capacity to support F-protein-based cell-cell fusion. To verify whether the effects monitored with a cell-cell fusion assay could be reproduced at the viral entry level, we transferred the four H genes with the single mutations completely abolishing SLAM-dependent fusion support activity into a plasmid coding for an infectious

TABLE 1. Solvent-exposed amino acids whose alpha-carbon atoms are predicted to be located within 10 Å from the alpha-carbon atoms of the anchor residues

Anchor	Nearby surface-exposed residues
CD46	
F431	A428, S429, L434, F476
V451	K445, N447, H448, N449, L464, N468
Y481	L464, N468, V478, S479, Q523
A527	I487, R547
SLAM	
Y529-D530	I487, T531, S532, V534, H536, R547
R533	I487, E492, D493, H495, P497, T531, S532, V534, H536
R553	T177, F549, Y551, F552, P554, F555, R556

MV genome. This infectious genome expresses a reporter GFP protein from an additional transcription unit (18), and therefore infected cells emit fluorescent green light when appropriately stimulated. In addition, the four mutations abolishing SLAM-dependent fusion support (Y529A, D530A, H533A, and Y553A) were combined into a single gene that was then transferred into the same MV genomic backbone. As a control, a protein predicted to have minimal CD46-dependent fusion support was constructed by transferring the V451S and A527S mutations into an H-protein wild-type coding region. This wild-type H protein was chosen because it supports less efficient entry into Vero cells than the vaccine strain H protein (31, 72). The corresponding gene was then transferred into the same MV genomic backbone as described above.

Viruses predicted to be SLAM blind were then recovered by the standard procedure based on the 293-3-46 helper cell line (60); the virus predicted to be CD46 blind was rescued by using the same cells overlaid with B95a cells (72). Stocks of standard and SLAM-blind viruses were prepared, and the titers were determined on Vero cells. Stocks of the CD46-blind virus were prepared, and titers were determined on Vero-SLAM cells (81); all viruses reached similar titers with similar kinetics, indicating that even the accumulation of multiple mutations had only minor effects on growth.

Vero (CD46 positive, SLAM negative) and B95a (CD46 negative, SLAM positive) simian cells were then infected at an MOI of 0.1, and the infection was allowed to proceed for 30 h on Vero cells or for 48 h on B95a cells, where syncytia formed more slowly. Figure 6A illustrates the progression of the infection in Vero (top row) and B95a cells (bottom row). In Vero cells infections with the five SLAM-blind mutants (from the right, Y529A, D530A, R533A, and Y533A and the four-way mutated virus) proceeded as efficiently as that of the control virus (H). In contrast, only a weakly positive small group of cells was detected in cells infected with H(wt)V451S,A527S. We note that this level of infection was weaker than that of a virus with a standard H(wt) protein (72). Infection progression was completely different in B95a cells (Fig. 6A, bottom row). None of the SLAM-blind viruses (five fields on the left) infected more than a few cells. Replication in these cells was efficient, but did not lead to the formation of syncytia. In contrast, syncytia covering more than half of the plate surface were scored in B95a cells infected with the SLAM entry competent control viruses: H or H(wt)V451S,A527S (Fig. 6A, bottom row, sixth and seventh fields). Mock-infected Vero and B95a cells were negative (Fig. 6A, last fields on the right, top and bottom rows).

We then lysed the cells that had been characterized by GFP analysis, prepared protein extracts, and analyzed the extracts by Western blot. As shown in Fig. 6B (top panel), in Vero cells all viruses with the exception of H(wt)V451S,A527S produced significant levels of H protein. The results were different in B95a cells, where only the two viruses that retained the competence to enter cells via SLAM [H and H(wt)451S,A527S, lanes 6 and 7] produced significant amounts of H protein. Taken together, these results indicate that the mutations identified by the cell-cell fusion assay exert their receptor-selective effect also in the context of a viral infection.

DISCUSSION

We have identified and located on a new structural model of the MV attachment protein residues that selectively interfere with fusion induced by either the immune-cell-specific (SLAM) or the ubiquitous (CD46) MV receptor. Based on these data, we have produced recombinant MVs that replicate selectively in cells expressing SLAM or CD46. Selectively receptor-blind viruses will be used to study MV spread, pathology, and immunosuppression and may have applications for the production of novel vaccines and therapeutics.

New structural model of MV H. After identifying several MV H-protein residues (anchors) crucial for SLAM-dependent fusion and others essential for CD46 (Vero cell receptor)-dependent fusion, we constructed an MV H structural model to allow more focused mutagenesis. This model is based on the sequence analysis of six morbillivirus H proteins and on the prediction of 18 structural motifs in these sequences. These motifs and secondary structure predictions were used to improve alignments of fold recognition servers, which identified the NDV HN ectodomain (13) as the best template. We used this final alignment to generate a structural model. We optimized the structure to minimize the energy and then used it to plan the next mutagenesis stage that identified a few additional residues interfering with receptor-specific fusion function (see below).

Previous studies of MV H-protein function have been interpreted based on another model that was developed by Langedijk et al. This model was based on multiple sequence alignments of a diverse set of neuraminidases, on the structure of the influenza virus neuraminidase, and on an intermediate model of a paramyxovirus HN (35). Comparison of the recently determined NDV HN structure with that of an influenza virus neuraminidase used by Langedijk et al. as a template gave a root mean square deviation of 2.17 Å for 222 carboxyl alpha atoms, indicating that, although the two enzymes share the same basic fold, there is considerable variation between them (13).

In view of these facts, it is not surprising that our model of MV H and that of Langedijk et al. differ in many aspects. Significantly, even the primary sequence alignments used to generate the models are different: the longest common stretch (51 residues) in the two alignments is situated in β-sheets 1 and 2. It comprises the secondary structure motifs d to f (Fig. 3, MASIA line, boxed) and covers a structural landmark of NDV

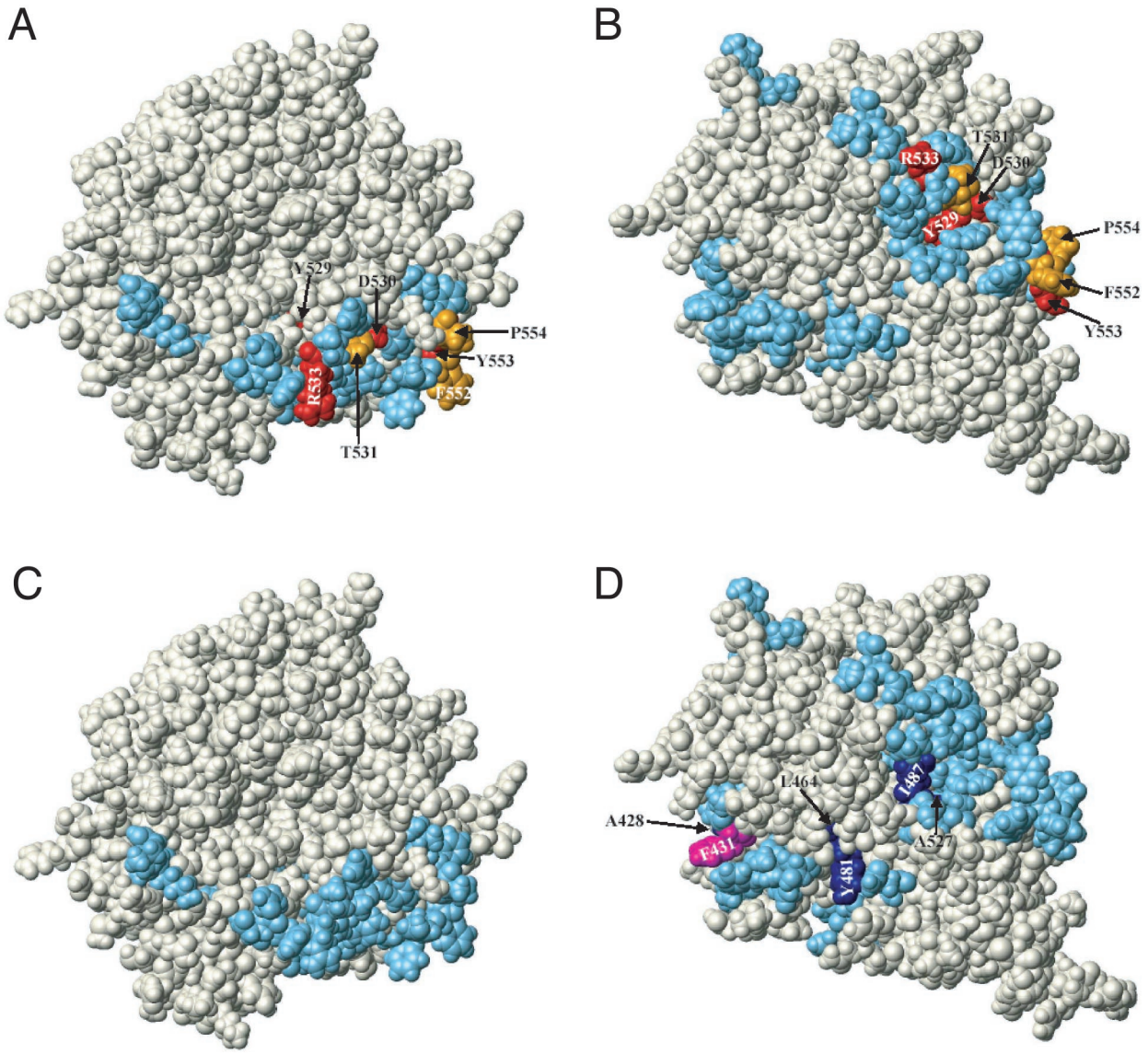

FIG. 5. Predicted location of all amino acids whose mutation reduces receptor-dependent fusion-support function on the new MV H-protein structural model. (A and C) Top views of the H molecule; (B and D) side views of the H molecule. (A and B) Residues whose mutation abolished SLAM-dependent fusion function are shown in red; those whose mutation strongly or moderately impaired SLAM-dependent fusion function are in gold. (C and D) The only residue whose mutation abolished CD46 (Vero cell)-dependent fusion is shown in pink; those whose mutation strongly or moderately impaired CD46-dependent fusion function are shown in dark blue. The ordinal number and chemical nature of all of the amino acids that selectively impaired fusion with any receptor are indicated. Residue V451, which strongly impaired CD46-dependent fusion, is located below the solvent-exposed surface.

H, motif e, which constitutes the most membrane-proximal part of the dimer interface in the globular head (13). Monomeric subunits of NDV HN interact back to back through this domain (12) that is situated opposite to the receptor binding sites we predict in MV H. Another motif (j) overlaps with the highly conserved H-protein "noose" epitope containing three cysteines (59). In contrast, the predicted neuraminidase catalytic site that Langedijk et al. located in a "funnel" on the top of the molecule and between the six β propeller sheets is absent from our model. The MV H protein is not known to have neuraminidase activity.

H amino acids relevant for receptor-induced fusion. In the MV H model all residues relevant for SLAM-dependent fusion map to two clusters located near each other around or above the protein midline in propeller sheet 5. Two of the four residues in one cluster are charged, whereas two of the three residues in the other are aromatic. The data recently published by the Yanagi group (73) suggest that two SLAM-binding clusters may exist in other morbilliviruses. The authors of that study grew CDV on B95a cells and noted that adaptation to simian SLAM resulted in mutation of H-protein residues 530 and 548, corresponding to MV H residues 534 and 552. As for

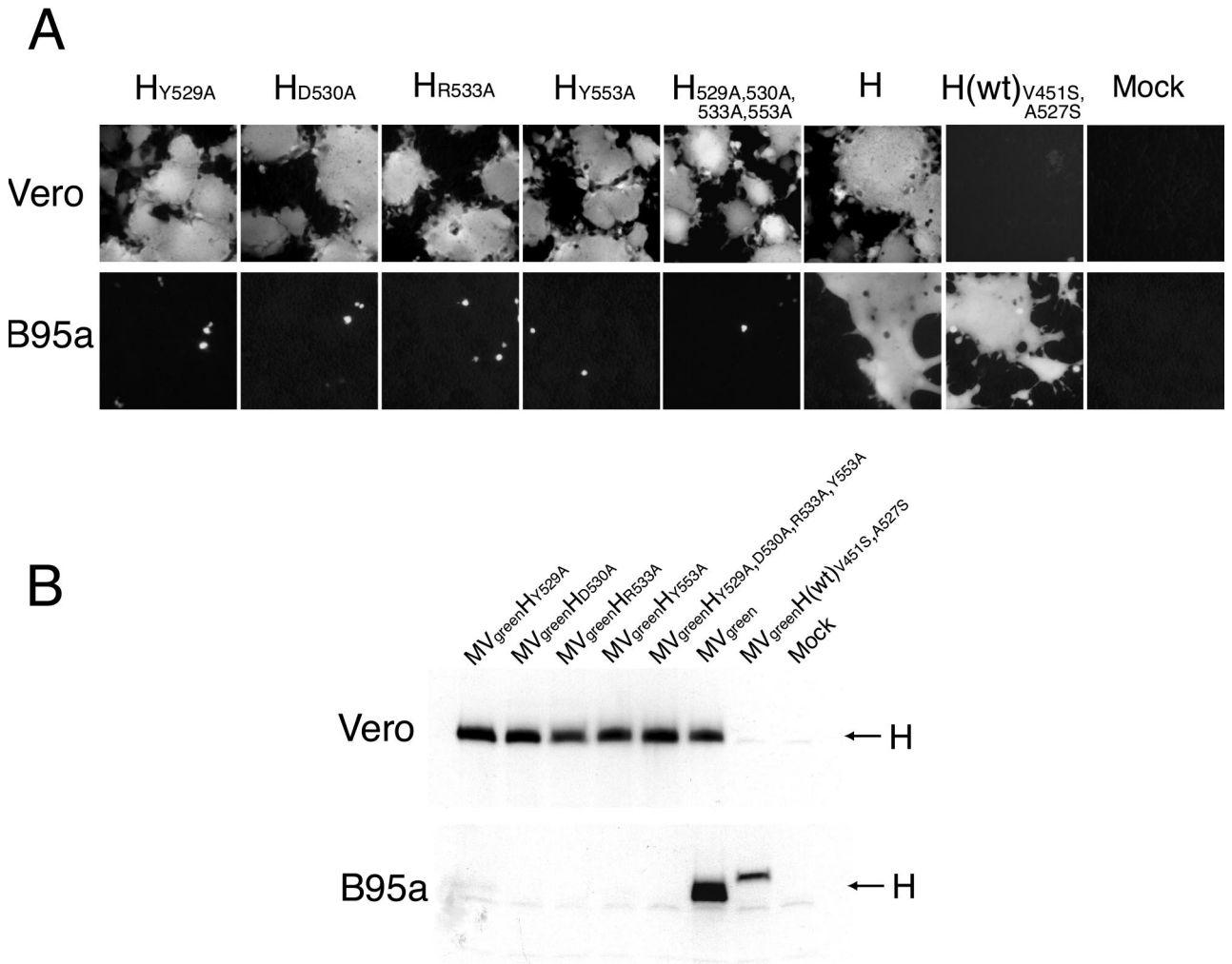

FIG. 6. Infection of Vero and B95a cells with selectively receptor-blind viruses. Green fluorescence emission of cells infected with different viruses (A) and analysis of H-protein production in the protein extracts of the same cells (B). Cells were infected with equivalent MOIs of the seven viruses indicated, photographed at 30 (Vero) or 48 (B95a) h postinfection, and lysed; protein extracts were prepared, and the expression of the H protein was analyzed by Western blot. All viruses had an identical genome, including the reporter protein GFP expressed from an additional transcription unit, and differed only in the H-protein amino acid(s) indicated. The H(wt)V451S,A527S protein, with two predicted additional glycosylation sites, migrates more slowly than all other proteins.

CD46, in the H model the three relevant residue clusters are located in or near the fourth propeller sheet. None of the CD46-relevant residues are charged, and a majority are apolar.

Paramyxovirus fusion may be triggered by receptor binding inducing conformational changes in the attachment protein (12, 79) that in turn elicit structural changes in the F protein (41, 64). Certain H-protein residues identified in the present study may be directly involved in receptor binding, others may support H-protein conformational changes necessary for signal transduction, and still others may promote or allow the F protein structural changes resulting in membrane fusion. Even if we cannot assign individual H amino acids to a specific function, the facts that all SLAM-relevant amino acids are predicted to be solvent exposed and can be sighted in a top view of the MV H model (Fig. 5A) are compatible with direct involvement in receptor binding: the MV envelope glycoproteins "spikes" (homooligomers) are tightly packed on the virus surface, and only the H-protein top may be directly available for receptor binding. On the other hand, none of the CD46-relevant residues can be sighted in a top view of the MV H model (Fig. 5C). It is conceivable that certain mutations, rather than directly affecting CD46 binding, modify lateral interactions of the spikes that facilitate receptor access. Moreover, certain SLAM- or CD46-relevant residues may support receptor-specific H-protein conformational changes that ultimately converge to elicit F-protein-mediated membrane fusion.

H-protein–receptor binding. To gain insights in the two receptor-dependent fusion processes, we are analyzing the binding of different pairs of mutated H-protein and receptor ectodomains. It is known that the association rate of the MV-Edm H-protein and SLAM ectodomains is very low (~3,000 $M^{-1}\,s^{-1}$), about 20 times lower than the association rate of the same protein with the CD46 ectodomain (66). However,

SLAM had a fivefold-lower dissociation rate from H than did CD46, indicating tighter binding.

Santiago et al. (66) observed that several monoclonal antibodies (74) completely inhibited binding of both CD46 and SLAM and suggested that the corresponding receptor binding surfaces may overlap. Hu et al. (29) characterized residues in the epitopes recognized by these monoclonal antibodies after sequencing MVs that escaped from their selective pressure; our model allows us to locate these residues. Two of the antibodies that completely inhibited binding to both receptors induced mutations near SLAM-relevant residues (F552 for I-41 and both S532 and R533 for 16-DE6), another (16-CD11) induced mutation of residue 491, situated between propeller sheets 4 and 5 but outside of the SLAM- or CD46-relevant residue clusters (for orientation, see residue E492 in Fig. 4C). I-44, an antibody that induced mutation of residue 189, partially inhibited binding to both receptors. Interestingly, this residue is predicted to be located on the surface between sheets 1 and 6. Moreover, I-29, an antibody inducing mutations of residues 313 and 314 predicted to be on the top of propeller sheet 2, completely inhibited binding of both receptors. Taken together, these results suggest that steric hindrance may in part explain the broad inhibitory effects observed by Santiago et al. Nevertheless, their suggestion that the SLAM- and CD46-binding surfaces may overlap is fully compatible with the results of our analysis. It should also be noted that our mutagenesis analysis focused on propeller sheets 4, 5, and 6 and that the effects of residues mapping on other sheets may have been missed.

Reciprocally, receptor amino acids essential for H-protein-supported fusion have been characterized. Several H-interacting residues were identified on CD46 (6), and their locations were predicted on a structural model of the two most membrane-distal domains (45). The subsequently obtained crystal structure of these domains confirmed the prediction that the H binding surface is located on the CD46 front side (7). It is not yet known which one of the MV H-protein residues interfering with CD46-dependent fusion are directly involved in binding but, once these are identified, docking of these two molecules will be modeled, and the predictions can be verified experimentally. As for the other receptor, recently SLAM residue H61 and its adjacent amino acids were shown to modulate cell fusion efficiency (49); a SLAM structure or structural model is necessary to support analogous in silico docking experiments with SLAM and MV H.

Selectively receptor-blind MV. SLAM-blind and CD46-blind MV will be used to investigate viral pathology: cell entry through both SLAM (81) and CD46 (32, 37, 50) may have a role in MV-induced immunosuppression. The limited competence of small animals, including transgenic mice expressing MV receptors, in sustaining efficient MV replication and pathology is an issue in the study of MV pathogenesis (22, 43, 48, 50, 63). Nevertheless, characterization of the properties of different recombinant viruses in a small animal model remains highly desirable before primate experimentation. Since MV and CDV have a very similar biology and pathology and an infectious cDNA of a CDV strain highly pathogenic for ferrets recently became available (84), we are currently systematically defining the SLAM-relevant residues of CDV H. Once SLAM-blind CDVs are recovered, their pathogenesis and immunosuppressive properties can be characterized in ferrets.

Receptor-blind viruses may be developed as more attenuated live vaccines for the protection of immunocompromized individuals (2, 17, 42) and derivatives thereof may find applications in cytoreductive therapy protocols based on the efficient replication of MV in cancer cells (21, 55–57). Moreover, recombinant MVs entering cells through targeted receptors have been produced (23, 71), and their efficacy in eliminating human cancer cell xenografts has been proven (5, 54). The prevention of entry through natural receptors will be combined with entry through targeted receptors to obtain fully retargeted MV. Phase I studies of the use of oncolytic MV in lymphoma and ovarian cancer are approved or in advanced planning (Adele Fielding and Evanthia Galanis, unpublished data), and future clinical trials may benefit from the use of retargeted viruses.

ACKNOWLEDGMENTS

We thank Adele Fielding, Mark Federspiel, Stephen Russell, and members of the Cattaneo laboratory for helpful discussions and Becky Sanford for excellent secretarial support.

This study was supported by NIH grant R01 CA90636 to R.C., grants from the Siebens and the Mayo Foundations to R.C., and a grant from the Department of Energy (DE-FG03-00ER63041) to W.B.

REFERENCES

1. **Altschul, S. F., T. L. Madden, A. A. Schaffer, J. Zhang, Z. Zhang, W. Miller, and D. J. Lipman.** 1997. Gapped BLAST and PSI-BLAST: a new generation of protein database search programs. Nucleic Acids Res. **25:**3389–3402.
2. **Angel, J. B., P. Walpita, R. A. Lerch, M. S. Sidhu, M. Masurekar, R. A. DeLellis, J. T. Noble, D. R. Snydman, and S. A. Udem.** 1998. Vaccine-associated measles pneumonitis in an adult with AIDS. Ann. Intern. Med. **129:**104–106.
3. **Bartz, R., U. Brinckmann, L. M. Dunster, B. Rima, V. Ter Meulen, and J. Schneider-Schaulies.** 1996. Mapping amino acids of the measles virus hemagglutinin responsible for receptor (CD46) downregulation. Virology **224:** 334–337.
4. **Borrow, P., and M. B. Oldstone.** 1995. Measles virus-mononuclear cell interactions. Curr. Top. Microbiol. Immunol. **191:**85–100.
5. **Bucheit, A. D., S. Kumar, D. Grote, Y. Lin, V. von Messling, R. Cattaneo, and A. K. Fielding.** 2003. An oncolytic measles virus engineered to enter cells through the CD20 antigen. Mol. Ther. **7:**62–72.
6. **Buchholz, C. J., D. Koller, P. Devaux, C. Mumenthaler, J. Schneider-Schaulies, W. Braun, D. Gerlier, and R. Cattaneo.** 1997. Mapping of the primary binding site of measles virus to its receptor CD46. J. Biol. Chem. **272:**22072–22079.
7. **Casasnovas, J. M., M. Larvie, and T. Stehle.** 1999. Crystal structure of two CD46 domains reveals an extended measles virus-binding surface. EMBO J. **18:**2911–2922.
8. **Cathomen, T., C. J. Buchholz, P. Spielhofer, and R. Cattaneo.** 1995. Preferential initiation at the second AUG of the measles virus F mRNA: a role for the long untranslated region. Virology **214:**628–632.
9. **Cathomen, T., H. Y. Naim, and R. Cattaneo.** 1998. Measles viruses with altered envelope protein cytoplasmic tails gain cell fusion competence. J. Virol. **72:**1224–1234.
10. **Cattaneo, R., and J. K. Rose.** 1993. Cell fusion by the envelope glycoproteins of persistent measles viruses which caused lethal human brain disease. J. Virol. **67:**1493–1502.
11. **Clements, C. J., and F. T. Cutts.** 1995. The epidemiology of measles: thirty years of vaccination, p. 13–33. *In* V. ter Meulen and M. A. Billeter (ed.), Measles virus. Springer-Verlag, Berlin, Germany.
12. **Corey, E. A., A. M. Mirza, E. Levandowsky, and R. M. Iorio.** 2003. Fusion deficiency induced by mutations at the dimer interface in the Newcastle disease virus hemagglutinin-neuraminidase is due to a temperature-dependent defect in receptor binding. J. Virol. **77:**6913–6922.
13. **Crennell, S., T. Takimoto, A. Portner, and G. Taylor.** 2000. Crystal structure of the multifunctional paramyxovirus hemagglutinin-neuraminidase. Nat. Struct. Biol. **7:**1068–1074.
14. **Cuff, J. A., and G. J. Barton.** 2000. Application of multiple sequence alignment profiles to improve protein secondary structure prediction. Proteins **40:**502–511.
15. **Cuff, J. A., M. E. Clamp, A. S. Siddiqui, M. Finlay, and G. J. Barton.** 1998.

JPred: a consensus secondary structure prediction server. Bioinformatics **14:**892–893.
16. **Dorig, R. E., A. Marcil, A. Chopra, and C. D. Richardson.** 1993. The human CD46 molecule is a receptor for measles virus (Edmonston strain). Cell **75:**295–305.
17. **Duclos, P., and B. J. Ward.** 1998. Measles vaccines: a review of adverse events. Drug Safety **19:**435–454.
18. **Duprex, W. P., S. McQuaid, L. Hangartner, M. A. Billeter, and B. K. Rima.** 1999. Observation of measles virus cell-to-cell spread in astrocytoma cells by using a green fluorescent protein-expressing recombinant virus. J. Virol. **73:**9568–9575.
19. **Erlenhoefer, C., W. J. Wurzer, S. Loffler, S. Schneider-Schaulies, V. ter Meulen, and J. Schneider-Schaulies.** 2001. CD150 (SLAM) is a receptor for measles virus but is not involved in viral contact-mediated proliferation inhibition. J. Virol. **75**:4499–4505.
20. **Fischer, D.** 2000. Hybrid fold recognition: combining sequence derived properties with evolutionary information. Pac. Symp. Biocomput. **5:**116–127.
21. **Grote, D., S. J. Russell, T. I. Cornu, R. Cattaneo, R. Vile, G. A. Poland, and A. K. Fielding.** 2001. Live attenuated measles virus induces regression of human lymphoma xenografts in immunodeficient mice. Blood **97:**3746–3754.
22. **Hahm, B., N. Arbour, D. Naniche, D. Homann, M. Manchester, and M. B. Oldstone.** 2003. Measles virus infects and suppresses proliferation of T lymphocytes from transgenic mice bearing human signaling lymphocytic activation molecule. J. Virol. **77:**3505–3515.
23. **Hammond, A. L., R. K. Plemper, J. Zhang, U. Schneider, S. J. Russell, and R. Cattaneo.** 2001. Single-chain antibody displayed on a recombinant measles virus confers entry through the tumor-associated carcinoembryonic antigen. J. Virol. **75:**2087–2096.
24. **Hasan, R. J., E. Pawelczyk, P. T. Urvil, M. S. Venkatarajan, P. Goluszko, J. Kur, R. Selvarangan, S. Nowicki, W. A. Braun, and B. J. Nowicki.** 2002. Structure-function analysis of decay-accelerating factor: identification of residues important for binding of the *Escherichia coli* Dr adhesin and complement regulation. Infect. Immun. **70:**4485–4493.
25. **Hashimoto, K., N. Ono, H. Tatsuo, H. Minagawa, M. Takeda, K. Takeuchi, and Y. Yanagi.** 2002. SLAM (CD150)-independent measles virus entry as revealed by recombinant virus expressing green fluorescent protein. J. Virol. **76:**6743–6749.
26. **Higgins, D. G., A. J. Bleasby, and R. Fuchs.** 1992. CLUSTAL V: improved software for multiple sequence alignment. Comput. Appl. Biosci. **8:**189–191.
27. **Hsu, E. C., C. Iorio, F. Sarangi, A. A. Khine, and C. D. Richardson.** 2001. CDw150(SLAM) is a receptor for a lymphotropic strain of measles virus and may account for the immunosuppressive properties of this virus. Virology **279:**9–21.
28. **Hsu, E. C., F. Sarangi, C. Iorio, M. S. Sidhu, S. A. Udem, D. L. Dillehay, W. Xu, P. A. Rota, W. J. Bellini, and C. D. Richardson.** 1998. A single amino acid change in the hemagglutinin protein of measles virus determines its ability to bind CD46 and reveals another receptor on marmoset B cells. J. Virol. **72:**2905–2916.
29. **Hu, A., H. Sheshberadaran, E. Norrby, and J. Kovamees.** 1993. Molecular characterization of epitopes on the measles virus hemagglutinin protein. Virology **192:**351–354.
30. **Hummel, K. B., J. A. Vanchiere, and W. J. Bellini.** 1994. Restriction of fusion protein mRNA as a mechanism of measles virus persistence. Virology **202:** 665–672.
31. **Johnston, I. C., V. ter Meulen, J. Schneider-Schaulies, and S. Schneider-Schaulies.** 1999. A recombinant measles vaccine virus expressing wild-type glycoproteins: consequences for viral spread and cell tropism. J. Virol. **73:** 6903–6915.
32. **Karp, C. L., M. Wysocka, L. M. Wahl, J. M. Ahearn, P. J. Cuomo, B. Sherry, G. Trinchieri, and D. E. Griffin.** 1996. Mechanism of suppression of cell-mediated immunity by measles virus. Science **273:**228–231.
33. **Kelley, L. A., R. M. MacCallum, and M. J. Sternberg.** 2000. Enhanced genome annotation using structural profiles in the program 3D-PSSM. J. Mol. Biol. **299:**499–520.
34. **Koradi, R., M. Billeter, and K. Wuthrich.** 1996. MOLMOL: a program for display and analysis of macromolecular structures. J. Mol. Graph. **14:**51–55.
35. **Langedijk, J. P., F. J. Daus, and J. T. van Oirschot.** 1997. Sequence and structure alignment of *Paramyxoviridae* attachment proteins and discovery of enzymatic activity for a morbillivirus hemagglutinin. J. Virol. **71:**6155–6167.
36. **Lecouturier, V., J. Fayolle, M. Caballero, J. Carabana, M. L. Celma, R. Fernandez-Munoz, T. F. Wild, and R. Buckland.** 1996. Identification of two amino acids in the hemagglutinin glycoprotein of measles virus (MV) that govern hemadsorption, HeLa cell fusion, and CD46 downregulation: phenotypic markers that differentiate vaccine and wild-type MV strains. J. Virol. **70:**4200–4204.
37. **Marie, J. C., J. Kehren, M. C. Trescol-Biemont, A. Evlashev, H. Valentin, T. Walzer, R. Tedone, B. Loveland, J. F. Nicolas, C. Rabourdin-Combe, and B. Horvat.** 2001. Mechanism of measles virus-induced suppression of inflammatory immune responses. Immunity **14:**69–79.
38. **Masse, N., T. Barrett, C. P. Muller, T. F. Wild, and R. Buckland.** 2002. Identification of a second major site for CD46 binding in the hemagglutinin protein from a laboratory strain of measles virus (MV): potential consequences for wild-type MV infection. J. Virol. **76:**13034–13038.
39. **Mathura, V., C. Schein, and W. Braun.** 2003. Identifying property-based sequence motifs in protein families and superfamilies: application to DNase I-related endonucleases. Bioinformatics **19:**1381–1390.
40. **Mathura, V. S., K. V. Soman, T. K. Varma, and W. Braun.** 2003. A multimeric model for murine anti-apoptotic protein BCL-2 and structural insights for its regulation by posttranslational modification. J. Mol. Model. **9:**298–303. [Online.]
41. **McGinnes, L. W., K. Gravel, and T. G. Morrison.** 2002. Newcastle disease virus HN protein alters the conformation of the F protein at cell surfaces. J. Virol. **76:**12622–12633.
42. **Moss, W. J., F. Cutts, and D. E. Griffin.** 1999. Implications of the human immunodeficiency virus epidemic for control and eradication of measles. Clin. Infect. Dis. **29:**106–112.
43. **Mrkic, B., J. Pavlovic, T. Rulicke, P. Volpe, C. J. Buchholz, D. Hourcade, J. P. Atkinson, A. Aguzzi, and R. Cattaneo.** 1998. Measles virus spread and pathogenesis in genetically modified mice. J. Virol. **72:**7420–7427.
44. **Mumenthaler, C., and W. Braun.** 1995. Automated assignment of simulated and experimental NOESY spectra of proteins by feedback filtering and self-correcting distance geometry. J. Mol. Biol. **254:**465–480.
45. **Mumenthaler, C., U. Schneider, C. J. Buchholz, D. Koller, W. Braun, and R. Cattaneo.** 1997. A 3D model for the measles virus receptor CD46 based on homology modeling, Monte Carlo simulations, and hemagglutinin binding studies. Protein Sci. **6:**588–597.
46. **Murtazina, D., A. V. Puchkaev, C. H. Schein, N. Oezguen, W. Braun, A. Nanavati, and I. A. Pikuleva.** 2002. Membrane-protein interactions contribute to efficient 27-hydroxylation of cholesterol by mitochondrial cytochrome P450 27A1. J. Biol. Chem. **277:**37582–37589.
47. **Naniche, D., G. Varior-Krishnan, F. Cervoni, T. F. Wild, B. Rossi, C. Rabourdin-Combe, and D. Gerlier.** 1993. Human membrane cofactor protein (CD46) acts as a cellular receptor for measles virus. J. Virol. **67:**6025–6032.
48. **Niewiesk, S.** 1999. Cotton rats (*Sigmodon hispidus*): an animal model to study the pathogenesis of measles virus infection. Immunol. Lett. **65:**47–50.
49. **Ohno, S., S. Fumio, N. Ono, and Y. Yanagi.** 2003. Histidine at position 61 and its adjacent amino acid residues are critical for the ability of SLAM (CD150) to act as a cellular receptor for measles virus. J. Gen. Virol. **84:**2381–2388.
50. **Oldstone, M. B., H. Lewicki, D. Thomas, A. Tishon, S. Dales, J. Patterson, M. Manchester, D. Homann, D. Naniche, and A. Holz.** 1999. Measles virus infection in a transgenic model: virus-induced immunosuppression and central nervous system disease. Cell **98:**629–640.
51. **Ono, N., H. Tatsuo, Y. Hidaka, T. Aoki, H. Minagawa, and Y. Yanagi.** 2001. Measles viruses on throat swabs from measles patients use signaling lymphocytic activation molecule (CDw150) but not CD46 as a cellular receptor. J. Virol. **75:**4399–4401.
52. **Outlaw, M. C., and C. R. Pringle.** 1995. Sequence variation within an outbreak of measles virus in the Coventry area during spring/summer 1993. Virus Res. **39:**3–11.
53. **Patterson, J. B., F. Scheiflinger, M. Manchester, T. Yilma, and M. B. Oldstone.** 1999. Structural and functional studies of the measles virus hemagglutinin: identification of a novel site required for CD46 interaction. Virology **256:**142–151.
54. **Peng, K.-W., K. A. Donovan, U. Schneider, R. Cattaneo, J. A. Lust, and S. J. Russell.** 2003. Oncolytic measles virus displaying a single chain antibody against CD38, a myeloma cell marker. Blood **101:**2557–2562.
55. **Peng, K. W., G. J. Ahmann, L. Pham, P. R. Greipp, R. Cattaneo, and S. J. Russell.** 2001. Systemic therapy of myeloma xenografts by an attenuated measles virus. Blood **98:**2002–2007.
56. **Peng, K. W., C. J. TenEyck, E. Galanis, K. R. Kalli, L. C. Hartmann, and S. J. Russell.** 2002. Intraperitoneal therapy of ovarian cancer using an engineered measles virus. Cancer Res. **62:**4656–4662.
57. **Phuong, L. K., C. Allen, K. W. Peng, C. Giannini, S. Greiner, C. J. TenEyck, P. K. Mishra, S. I. Macura, S. J. Russell, and E. C. Galanis.** 2003. Use of a vaccine strain of measles virus genetically engineered to produce carcinoembryonic antigen as a novel therapeutic agent against glioblastoma multiforme. Cancer Res. **63:**2462–2469.
58. **Plemper, R., A. Hammond, and R. Cattaneo.** 2000. Characterization of a region of measles virus hemagglutinin sufficient for its dimerization. J. Virol. **74:**6485–6493.
59. **Putz, M. M., J. Hoebeke, W. Ammerlaan, S. Schneider, and C. P. Muller.** 2003. Functional fine-mapping and molecular modeling of a conserved loop epitope of the measles virus hemagglutinin protein. Eur. J. Biochem. **270:** 1515–1527.
60. **Radecke, F., P. Spielhofer, H. Schneider, K. Kaelin, M. Huber, C. Dotsch, G. Christiansen, and M. A. Billeter.** 1995. Rescue of measles viruses from cloned DNA. EMBO J. **14:**5773–5784.
61. **Rager, M., S. Vongpunsawad, W. P. Duprex, and R. Cattaneo.** 2002. Polyploid measles virus with hexameric genome length. EMBO J. **21:**2364–2372.
62. **Rima, B. K., J. A. Earle, K. Baczko, V. ter Meulen, U. G. Liebert, C. Carstens, J. Carabana, M. Caballero, M. L. Celma, and R. Fernandez-**

Munoz. 1997. Sequence divergence of measles virus haemagglutinin during natural evolution and adaptation to cell culture. J. Gen. Virol. **78:**97–106.
63. **Roscic-Mrkic, B., R. A. Schwendener, B. Odermatt, A. Zuniga, J. Pavlovic, M. A. Billeter, and R. Cattaneo.** 2001. Roles of macrophages in measles virus infection of genetically modified mice. J. Virol. **75:**3343–3351.
64. **Russell, C. J., T. S. Jardetzky, and R. A. Lamb.** 2001. Membrane fusion machines of paramyxoviruses: capture of intermediates of fusion. EMBO J. **20:**4024–4034.
65. **Sanner, M., A. Widmer, H. Senn, and W. Braun.** 1989. GEOM: a new tool for molecular modeling based on distance geometry calculations with NMR data. J. Comput. Aided Mol. Des. **3:**195–210.
66. **Santiago, C., E. Bjorling, T. Stehle, and J. M. Casasnovas.** 2002. Distinct kinetics for binding of the CD46 and SLAM receptors to overlapping sites in the measles virus hemagglutinin protein. J. Biol. Chem. **277:**32294–32301.
67. **Sato, T. A., M. Enami, and T. Kohama.** 1995. Isolation of the measles virus hemagglutinin protein in a soluble form by protease digestion. J. Virol. **69:**513–516.
68. **Schaffer, A. A., L. Aravind, T. L. Madden, S. Shavirin, J. L. Spouge, Y. I. Wolf, E. V. Koonin, and S. F. Altschul.** 2001. Improving the accuracy of PSI-BLAST protein database searches with composition-based statistics and other refinements. Nucleic Acids Res. **29:**2994–3005.
69. **Schaumann, T., W. Braun, and K. Wuthrich.** 1990. The program FANTOM for energy refinement of polypeptides and proteins using a Newton-Raphson minimizer in torsion angle space. Biopolymers **29:**679–694.
70. **Schein, C. H., G. T. Nagle, J. S. Page, J. V. Sweedler, Y. Xu, S. D. Painter, and W. Braun.** 2001. Aplysia attractin: biophysical characterization and modeling of a water-borne pheromone. Biophys. J. **81:**463–472.
71. **Schneider, U., F. Bullough, S. Vongpunsawad, S. J. Russell, and R. Cattaneo.** 2000. Recombinant measles viruses efficiently entering cells through targeted receptors. J. Virol. **74:**9928–9936.
72. **Schneider, U., V. von Messling, P. Devaux, and R. Cattaneo.** 2002. Efficiency of measles virus entry and dissemination through different receptors. J. Virol. **76:**7460–7467.
73. **Seki, F., N. Ono, R. Yamaguchi, and Y. Yanagi.** 2003. Efficient isolation of wild strains of canine distemper virus in Vero cells expressing canine SLAM (CD150) and their adaptability to marmoset B95a cells. J. Virol. **77:**9943–9950.
74. **Sheshberadaran, H., and E. Norrby.** 1986. Characterization of epitopes on the measles virus hemagglutinin. Virology **152:**58–65.
75. **Shibahara, K., H. Hotta, Y. Katayama, and M. Homma.** 1994. Increased binding activity of measles virus to monkey red blood cells after long-term passage in Vero cell cultures. J. Gen. Virol. **75:**3511–3516.
76. **Soman, K. V., C. H. Schein, H. Zhu, and W. Braun.** 2001. Homology modeling and simulations of nuclease structures. Methods Mol. Biol. **160:**263–286.
77. **Soman, K. V., and W. Braun.** 2001. Determining the three-dimensional fold of a protein from approximate constraints: a simulation study. Cell Biochem. Biophys. **34:**283–304.
78. **Soman, K. V., T. Midoro-Horiuti, J. C. Ferreon, R. M. Goldblum, E. G. Brooks, A. Kurosky, W. Braun, and C. H. Schein.** 2000. Homology modeling and characterization of IgE binding epitopes of mountain cedar allergen Jun a3. Biophys. J. **79:**1601–1609.
79. **Takimoto, T., G. L. Taylor, H. C. Connaris, S. J. Crennell, and A. Portner.** 2002. Role of the hemagglutinin-neuraminidase protein in the mechanism of paramyxovirus-cell membrane fusion. J. Virol. **76:**13028–13033.
80. **Tatsuo, H., N. Ono, K. Tanaka, and Y. Yanagi.** 2000. SLAM (CDw150) is a cellular receptor for measles virus. Nature **406:**893–897.
81. **Tatsuo, H., N. Ono, and Y. Yanagi.** 2001. Morbilliviruses use signaling lymphocyte activation molecules (CD150) as cellular receptors. J. Virol. **75:**5842–5850.
82. **Thompson, J. D., D. G. Higgins, and T. J. Gibson.** 1994. CLUSTAL W: improving the sensitivity of progressive multiple sequence alignment through sequence weighting, position-specific gap penalties and weight matrix choice. Nucleic Acids Res. **22:**4673–4680.
83. **Venkatarajan, M., and W. Braun.** 2001. New quantitative descriptors of amino acids based on multidimensional scaling of a large number of physical-chemical properties. J. Mol. Model. **7:**445–453.
84. **von Messling, V., C. Springfeld, P. Devaux, and R. Cattaneo.** 2003. A ferret model of canine distemper virus virulence and immunosuppression. J. Virol. **77:**12579–12591.
85. **Wild, T. F., E. Malvoisin, and R. Buckland.** 1991. Measles virus: both the haemagglutinin and fusion glycoproteins are required for fusion. J. Gen. Virol. **72:**439–442.
86. **Zhu, H., and W. Braun.** 1999. Sequence specificity, statistical potentials, and three-dimensional structure prediction with self-correcting distance geometry calculations of beta-sheet formation in proteins. Protein Sci. **8:**326–342.
87. **Zhu, H., C. Schein, and W. Braun.** 1999. Homology modeling and molecular dynamics simulations of PBCV-1 glycosylase complexed with UV-damaged DNA. J. Mol. Model. **5:**302–316.
88. **Zhu, H., C. H. Schein, and W. Braun.** 2000. MASIA: recognition of common patterns and properties in multiple aligned protein sequences. Bioinformatics **16:**950–951.